

pubs.acs.org/est Article

Unraveling the Mechanisms of Fe Oxidation and Mn Reduction on Mn Indicators of Reduction in Soil (IRIS) Films

Matt A. Limmer, Franklin A. Linam, Abby E. Evans, and Angelia L. Seyfferth*



Cite This: Environ. Sci. Technol. 2023, 57, 6530-6539



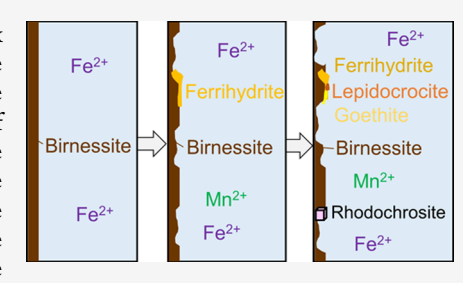
ACCESS

III Metrics & More

Article Recommendations

Supporting Information

ABSTRACT: Indicators of reduction in soil (IRIS) devices are low-cost soil redox sensors coated with Fe or Mn oxides, which can be reductively dissolved from the device under suitable redox conditions. Removal of the metal oxide coating from the surface, leaving behind the white film, can be quantified and used as an indicator of reducing conditions in soils. Manganese IRIS, coated with birnessite, can also oxidize Fe(II), resulting in a color change from brown to orange that complicates the interpretation of coating removal. Here, we studied field-deployed Mn IRIS films where Fe oxidation was present to unravel the mechanisms of Mn oxidation of Fe(II) and the resulting minerals on the IRIS film surface. We observed reductions in the Mn average



oxidation state when Fe precipitation was evident. Fe precipitation was primarily ferrihydrite (30-90%), but lepidocrocite and goethite were also detected, notably when the Mn average oxidation state decreased. The decrease in the average oxidation state of Mn was due to the adsorption of Mn(II) to the oxidized Fe and the precipitation of rhodochrosite $(MnCO_3)$ on the film. The results were variable on small spatial scales (<1 mm), highlighting the suitability of IRIS in studying heterogeneous redox reactions in soil. Mn IRIS also provides a tool to bridge lab and field studies of the interactions between Mn oxides and reduced constituents.

KEYWORDS: birnessite, ferrihydrite, lepidocrocite, goethite, synchrotron X-ray absorption spectroscopy, rhodochrosite

■ INTRODUCTION

Redox reactions control the fate and transport of many elements in soil, including several essential plant nutrients and environmental contaminants. However, accurate measurements of redox potentials in soil are often difficult to perform, require expensive equipment, and/or fail to capture the spatial and temporal heterogeneity in soil.² Environmental redox regimes are typically viewed from the perspective of terminal electron acceptors, including oxygen, nitrate, manganese (Mn), iron (Fe), sulfate, and carbon dioxide. For both Mn and Fe, the oxidized forms are practically insoluble, while the reduced forms are more soluble.³ Utilizing these redox reactions, indicators of reduction in soil (IRIS) devices were developed as a low-cost, in situ technique for observing reducing conditions in soil.4-6 IRIS first used Fe oxides (ferrihydrite and goethite) coated on a PVC pipe. Under Fe-reducing conditions, the orange Fe coating reductively dissolves from the device, revealing the white PVC underneath. This coating removal is correlated with the extent and location of Fe reduction⁸⁻¹⁰ and has been included as a criterion for identifying hydric soils.¹¹ Additionally, Fe IRIS devices have been used to monitor sulfidic environments through the formation of FeS, a sparingly soluble, black compound that rapidly forms when hydrogen sulfide is present. 12,13 To observe Mn-reducing conditions, various iterations of dark brown, birnessite coatings have been developed for IRIS, 14-16 which reductively dissolves under Mn-reducing conditions. Collectively, these IRIS devices allow for low-cost spatial and/or

temporal monitoring for some of the most common redoxsensitive elements in soils.

Manganese IRIS devices are of interest due to the relatively high soil redox potentials at which Mn reduction occurs. Nitrate, a plant nutrient and groundwater contaminant, can be reduced under similar redox conditions as Mn oxides. However, monitoring nitrate reduction in time and space is complex, and Mn IRIS has been proposed as a proxy for measuring nitrate reduction. Manganese IRIS devices are also more sensitive to suboxic conditions than Fe IRIS due to the higher soil redox potentials under which Mn reduction occurs relative to Fe reduction. Studies in the field and the laboratory have also shown that Mn coating removal occurs more quickly than Fe coating removal. Manganese IRIS may also be valuable in demonstrating reducing conditions at locations where Fe reduction is unfavorable, such as calcareous soils that can have higher redox potentials due to higher pH. 16

While Mn IRIS devices can demonstrate Mn-reducing conditions through coating removal, they can also accumulate Fe oxides, hydroxides, and oxyhydroxides (hereafter simply referred to as "oxides") on the surface because birnessite can

Received: January 6, 2023 Revised: April 1, 2023 Accepted: April 3, 2023 Published: April 13, 2023





oxidize aqueous Fe(II).²² Precipitation of Fe oxides onto Mn IRIS devices is relatively common where porewater Fe(II) is present.^{15,23} This presence of oxidized Fe on Mn IRIS has been attributed to the ability of birnessite to oxidize $Fe(II)^{15}$ through the reaction

$$MnO_2 + 2Fe^{2+} + 4H_2O \rightarrow Mn^{2+} + 2Fe(OH)_3 + 2H^+$$
(1)

Accumulation of such Fe oxides on Mn IRIS films appears as an orange color, resembling an Fe IRIS film that had been coated with synthetic Fe oxides, yet the Fe oxides are formed in situ or "neoformed". Extractions and spectroscopy have confirmed that these orange-colored deposits contain Fe. 18,21,24 However, deposition of Fe on Mn IRIS films is not universally observed: Stiles et al. 16 did not observe any orange staining on Mn IRIS films at a site where Fe IRIS did not show coating removal. Others have reported relatively minor orange staining on Mn IRIS.¹⁹ Fe staining has also occurred on IRIS films after Mn-coating removal. Short-range ordered Fe oxides have been observed on Mn IRIS in a soil subjected to three different temperatures; however, Fe deposits only appeared at the water table and after the Mn was removed, suggesting oxidation of Fe(II) by oxygen. 20 Fe oxides have also been found on uncoated IRIS films adjacent to rice rhizospheres, resulting in root-shaped Fe oxide deposits due to the oxidation of Fe(II) by root radial oxygen loss. 25,2

Past work has established that deposition of neoformed Fe oxides on Mn IRIS films varies between and within soils, and variations in colors formed on the IRIS film after deployment suggest that complex geochemistry occurs on the surface. It is crucial to better understand the fate of Mn and Fe on IRIS films when used as passive sensors of reducing conditions and as possible samplers of associated trace elements. To our knowledge, a comprehensive understanding of the mechanisms of coupled Mn reduction of field-deployed Mn IRIS and Fe(II) oxidation has not been conducted. The objectives of this work were, therefore, to characterize the spatial variability in Mn(III, IV) oxidation of Fe(II), identify the resulting Fe(III) minerals, and observe the mechanisms of how Mn(III, IV) is reduced under field conditions by Fe(II). To accomplish these objectives, we analyzed paddy field-deployed Mn IRIS films with Mn and Fe synchrotron X-ray absorption spectroscopy (XAS) at the millimeter scale (i.e., bulk scale), at the micron scale coupled to X-ray fluorescence (μ XRF) imaging, and via SEM and XRD.

■ MATERIALS AND METHODS

Mn IRIS Films. Manganese IRIS films were coated using published methods. ¹⁴ Briefly, sodium lactate and potassium permanganate were combined at a molar ratio of 6.7 and stirred for 2 h. After centrifuging and washing, the solids were dialyzed for 3 days. The Mn coating was applied to white, rigid vinyl films (RVW1018, Coast to Coast Label, Fountain Valley, CA). ²⁷ The films were cut to 7.5 cm \times 30.5 cm.

Manganese IRIS films were placed into flooded rice paddies at the University of Delaware. These 2 m \times 2 m rice paddies were densely planted with rice and were monitored weekly for porewater chemistry using rhizon samplers and were managed using alternate wetting and drying (AWD). The soil (Ultisol/Acrisol) is an Elsinboro silty clay loam and had a pH of 6.3 (1:1 water:soil) and organic matter of 1.5% measured by loss on ignition. Mehlich-3-extractable Mn and Fe were 140 and 306 mg/kg, respectively. Reducible Fe was

measured by sequential extraction, with 2.2 g/kg of short-range ordered Fe oxides and 12.5 g/kg crystalline Fe oxides.³⁰ The soil reducible Mn was 180 mg/kg as extracted by 0.1 M hydroxylamine hydrochloride and 0.01 M nitric acid.³¹ Porewater was collected every ~7 days using a rhizon sampler (1910, Soil Moisture Corp. Goleta, CA) and a vacuum syringe. Rhizons were placed ~15 cm below the ground surface and were within 0.5 m of all IRIS films. Porewater was immediately measured using calibrated probes for pH and redox potential (Ag/AgCl electrode, values reported relative to the standard hydrogen electrode). Reduced Fe was measured colorimetrically using the ferrozine method, 32 and porewater Mn was measured colorimetrically after oxidation to permanganate.³¹ A total of 108 IRIS films were deployed in 18 rice paddies during the reproductive growth phase (six films per paddy). Each film was installed into a 2.5-cm-diameter soil core hole so that the top of the film was flush with the soil surface. The films were installed at the beginning of a dry down cycle in part to study how Mn IRIS reacted to changing redox conditions during dry down. After 3 days, the water table reached the target depth of 15 cm, and the paddies were reflooded and remained flooded. An IRIS film was removed from each flooded paddy every 2-4 days until all of the films were removed by 20 days. Iron precipitation was observed on 99% of the films. Four films (labeled 1-4, Figure S1 and Table S1) were selected for further study using synchrotron radiation, SEM, and XRD (described below). Selection criteria included selecting (1) films with a range of exposure durations and porewater Fe and Mn concentrations (Table S1), (2) films that contained areas where Mn appeared to dominate, areas where Fe appeared to dominate, and areas where Fe and Mn were mixed (Figure S1), and (3) films that differed in patterns of Mn and Fe with depth. Through the selection of these films, we aimed to capture a wide range of conditions over which Mn and Fe interacted in this system.

Synchrotron μ XRF and μ XAS. Select areas of the films were analyzed at the Stanford Synchrotron Radiation Lightsource (SSRL) at beamline 2–3. At this beamline, the incident beam was focused to ~2 μ m, and the sample was mounted at 45° relative to the incident beam. Fluorescent X-rays were measured using a vortex silicon drift detector mounted at 90° relative to the incident beam. Manganese and Fe K_{α} and K_{β} fluorescence lines were the dominant fluorescent X-rays measured. The sample was rastered across the beam using a step size of 5 μ m × 5 μ m and a dwell time of 20 ms/pixel. The incident beam energy was 7200 eV for μ XRF imaging. Data were processed in SMAK v2.0, 33 and the X-ray fluorescence spectra were refit using the PyMCA module in SMAK to correct for potential interference between the Fe K_{β} emission line and the Mn K_{α} emission line.

At selected locations on the μ XRF map, Mn microprobe X-ray absorption near-edge structure (μ XANES) spectra were acquired to determine the oxidation state of Mn on the films. The first inflection point of a Mn foil was calibrated to 6539.0 eV. The μ XANES scans were performed in duplicate, and spectra were averaged, normalized, and background-subtracted using Athena v0.9.26. Linear combination fitting (LCF) was used to determine the Mn oxidation state following the combo method of Manceau et al.³⁴ Using this method, the derivative of the normalized and background-subtracted Mn XANES spectra was fit using the following pure oxidation state standards: ramsdellite (IV), birnessite (IV), manganite (III), Mn₂O₃ (III), groutite (III), MnSO_{4(aq)} (II), and tephroite

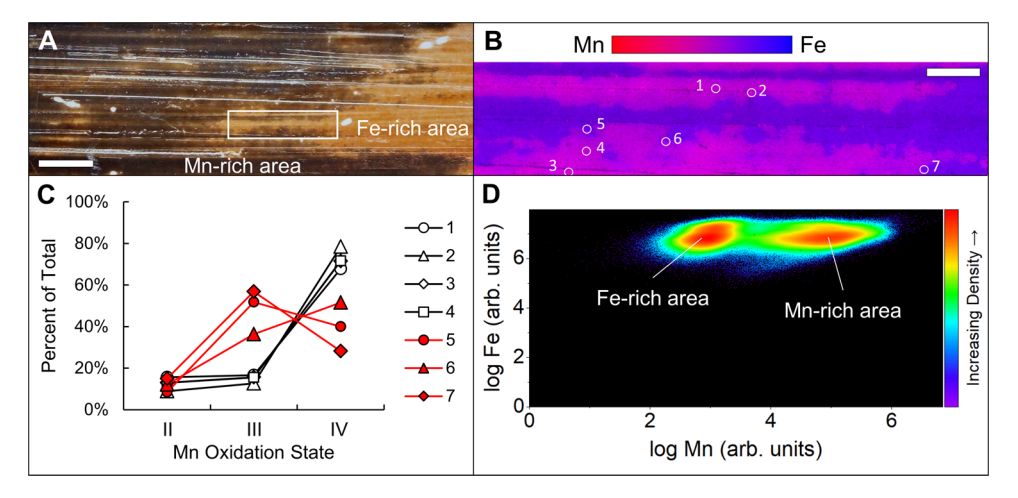


Figure 1. Manganese IRIS film 1 shows partial reduction of Mn oxides that coincide with Mn–Fe transition zones. (A) Image of films, with area analyzed by synchrotron μ XRF shown in the white rectangle. The scale bar is 5 mm. Full film shown in Figure S1. (B) Synchrotron μ XRF false bicolor plot showing the presence of Fe and Mn. Numbered locations were analyzed by Mn μ XANES spectroscopy. The scale bar is 1 mm. (C) Linear combination fitting of Mn μ XANES spectra showing the proportion of oxidation states present at each location. Locations are generally colored according to the dominant Mn oxidation state present. (D) Density correlation plot of pixels in panel B.

(II).³⁴ When performing the LCF, the fit was not constrained to sum to 1 because the problem is mathematically overconstrained. The proportion of each fit species was used to calculate the fraction of each oxidation state present and the Mn average oxidation state (AOS).

Bulk Mn XANES, Mn EXAFS, and Fe EXAFS Spectroscopy, XRD, and SEM. Selected areas of the Mn IRIS films were also analyzed at the National Synchrotron Light Source (NSLS-II) on 6-BM (BMM) for Mn XANES, Mn extended Xray absorption fine structure (EXAFS), and Fe EXAFS spectroscopy. Slits were approximately 1 mm \times 5 mm, although the width was adjusted to avoid excessive fluorescence counts. Manganese XAS was performed using a four-element vortex silicon drift detector, while Fe EXAFS spectra were collected in transmission. The energy was scanned from 200 eV below the edge to $k = 15 \text{ Å}^{-1}$ (Fe) or $k = 11.5 \text{ Å}^{-1}$ (Mn), with steps of 0.05 Å⁻¹ and an integration time of 1 s in the EXAFS region. Three replicate scans were measured and averaged prior to background subtraction and normalization. Manganese XANES spectroscopy followed the LCF method described for μ XANES spectroscopy (above). Manganese EXAFS spectra were extracted using an E₀ of 6545.7 eV, which corresponded to the peak of the first inflection point for Mn(II) adsorbed onto ferrihydrite (FHY). Initial standards included a nonreacted (aboveground) section of a Mn IRIS film and 2% by weight Mn(II) adsorbed onto FHY. Linear combination fitting of the k^3 weighted spectra from k of 2-8 Å⁻¹ revealed poor fits for many films. The database of Manceau et al., 34 as well as samples of Mn(III) coprecipitated in lepidocrocite³⁵ and Mn(III) coprecipitated in goethite³⁶ were used to explore potential additional Mn minerals to be added to the linear combination fitting (see the SI for more details on these synthesized minerals). Rhodochrosite (MnCO₃) consistently fit well and was added to the LCF and was later confirmed by SEM and XRD. Fe EXAFS spectra were calibrated to 7112.0 eV for the first inflection point of an Fe foil. The background-subtracted and normalized spectra were fit using k^3 weighting from k of 2–12 Å⁻¹. Normalized Mn and Fe spectra for samples and standards are available as text files in the SI. The standards used in the fitting were 2-line ferrihydrite, lepidocrocite (LEP), and

goethite (GOE). X-ray diffraction (XRD) was performed on sections of IRIS films using a Bruker D8 diffractometer (Cu $K_{\alpha 1}$), with the 2θ angle scanned from 15 to 60° . The IRIS films were directly analyzed without any preparation. Films analyzed included a blank, uncoated film, a film coated with Mn, a film where Fe oxides were dominant, and films where Mn EXAFS LCF identified rhodochrosite. Films were imaged using a scanning electron microscope (Apreo VolumeScope SEM) after coating with platinum.

■ RESULTS

Film Descriptive Statistics. The average area of the \sim 107 Mn films covered with Fe precipitation was 22% of the film (standard deviation 16%). No significant trends in Fe deposition over time were observed. The four selected films for further investigation, hereafter referred to as Mn IRIS films 1–4, generally had more Fe precipitation on the film than average and were exposed to Fe-reducing conditions (Table S1). On average, porewater redox potentials, Fe(II) concentrations, and Mn concentrations ranged from 44 to 110 mV, 270 to 830 μ M, and 320 to 580 μ M, respectively (Table S1).

Elemental Mapping and Mn μ XANES Spectroscopy. Manganese IRIS film 1 showed Fe staining collocated with reduction of Mn oxides (Figure S1). Areas dark brown in color were termed "Mn-rich areas" and presumed to contain predominantly Mn oxides. Orange deposits, termed "Fe-rich areas", were apparent in the scanned image of the IRIS film (Figure 1A), and these deposits were verified to contain Fe through μ XRF imaging (Figures 1B and S2). However, even areas where Mn was abundant showed amounts of Fe similar to areas where Mn was no longer dominant (Figure 1D). In Mn-rich areas (spots 1-4 in Figure 1C), μXANES spectra revealed that Mn(IV) was the predominant oxidation state (Table S2). The Mn amount was too limited in Fe-rich areas for μ XANES spectroscopy, but spots 5–7 located at the interface of the Fe- and Mn-rich areas showed reduction to Mn(III). All measured spots on Mn IRIS film 1 showed negligible Mn(II).

Manganese IRIS film 2 showed a Mn-rich area adjacent to an Fe-rich area, with an interface zone between the two that appeared lighter in color (Figure 2A). The false bicolor plot

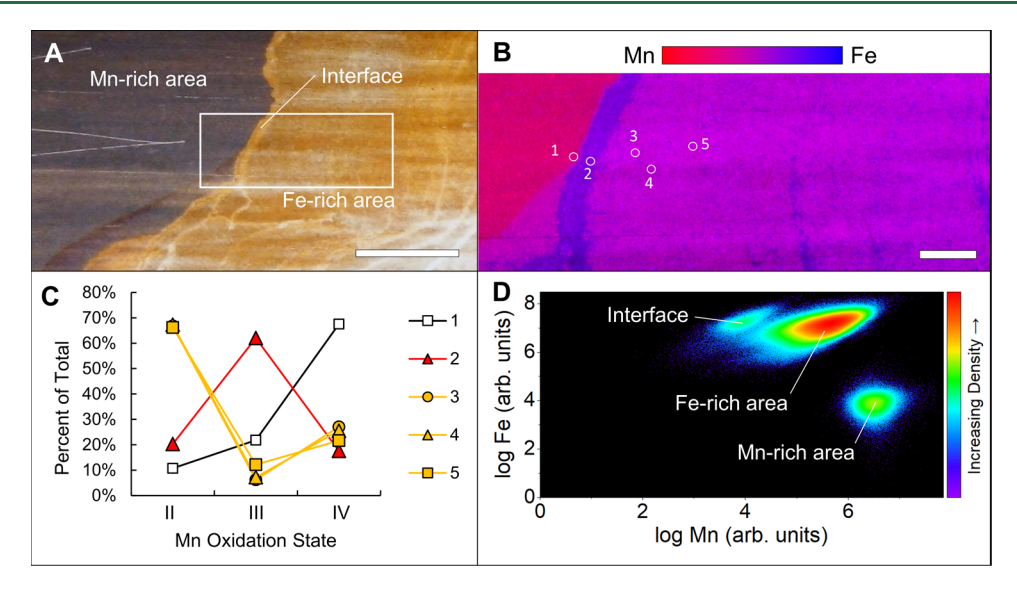


Figure 2. Manganese IRIS film 2 shows a nearly complete reduction of Mn oxides in the Fe-rich area. (A) Image of films, with area analyzed by synchrotron μ XRF shown in the white rectangle. The scale bar is 5 mm. Full film shown in Figure S1. (B) Synchrotron μ XRF false bicolor plot showing the presence of Fe and Mn. Numbered locations were analyzed by Mn μ XANES spectroscopy. The scale bar is 1 mm. (C) Linear combination fitting of Mn μ XANES spectra showing the proportion of oxidation states present at each location. Locations are colored according to the dominant Mn oxidation state present. (D) Density correlation plot of pixels in panel (B).

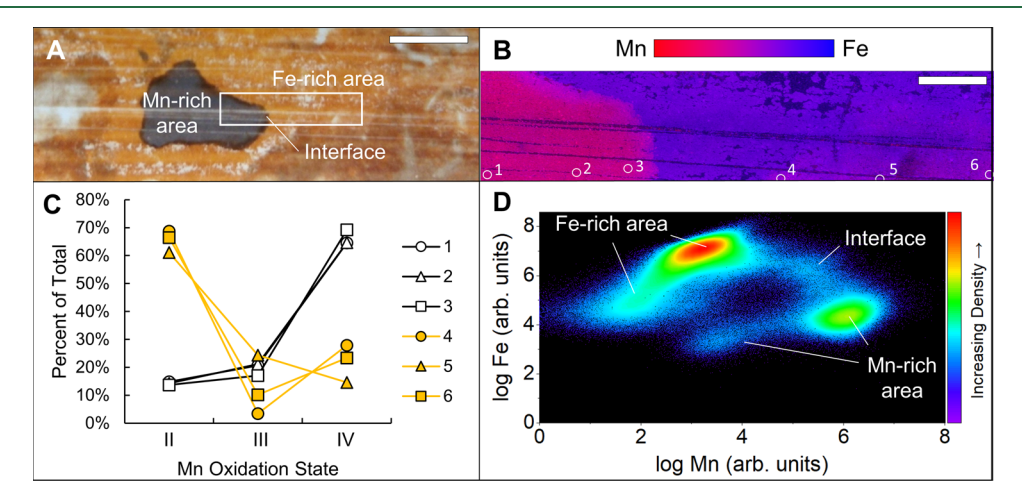


Figure 3. Manganese IRIS film 3 shows a nearly complete reduction of Mn oxide in the Fe-rich area. (A) Image of films, with area analyzed by synchrotron μ XRF shown in the white rectangle. The scale bar is 5 mm. Full film shown in Figure S1. (B) Synchrotron μ XRF false bicolor plot showing the presence of Fe and Mn. Numbered locations were analyzed by Mn μ XANES spectroscopy. The scale bar is 1 mm. (C) Linear combination fitting of Mn μ XANES spectra showing the proportion of oxidation states present at each location. Locations are colored according to the dominant Mn oxidation state present. (D) Density correlation plot of pixels in panel (B).

showed low amounts of Fe in most of the Mn-rich area, while the Fe-rich area contained both Fe and Mn (Figures 2B and S3). In contrast, the interface area had less Mn than the Fe-rich area (Figure 2D). The Mn μ XANES spectra showed a progression of Mn(IV) to Mn(III) to Mn(II) in the Mn-rich, interface, and Fe-rich areas, respectively (Figure 2C and Table S2).

Manganese IRIS film 3 appeared similar to Mn IRIS film 2, although the interface area was less distinct (Figure 3A). The false bicolor plot showed a stronger separation of Mn and Fe than the other films, with the Mn-rich area dominated by Mn and the Fe-rich area containing a mixture of Fe and Mn (Figures 3B and Figure S4). This pattern is also evident in the elemental density correlation plot, where the Fe-rich area has much lower Mn amounts than the Mn-rich area, particularly compared to the other IRIS films (Figure 3D). Note that the

smearing of the data toward the graph origin represents areas on the film where the coating was abraded away during film removal or microbially removed (i.e., white areas). While the Mn-rich area was dominated by Mn(IV), the Fe-rich area was dominated by Mn(II) (Figure 3C and Table S2).

Bulk Mn XANES, Mn EXAFS, and Fe EXAFS Spectroscopy. Select locations on the four films were analyzed to determine how Mn reduction was coupled with Fe oxidation. Locations numbered 1 represent areas dominated by Mn (Figure 4A). Other locations of interest included interface areas between Mn- and Fe-rich areas (e.g., film 3, location 2), Fe-rich areas (e.g., film 4, location 3), areas of mixed Mn and Fe (e.g., film 2, location 3), and areas where the remaining Mn appears light in color (e.g., film 4, location 4). At each location, Mn XANES, Mn EXAFS, and Fe EXAFS spectra were

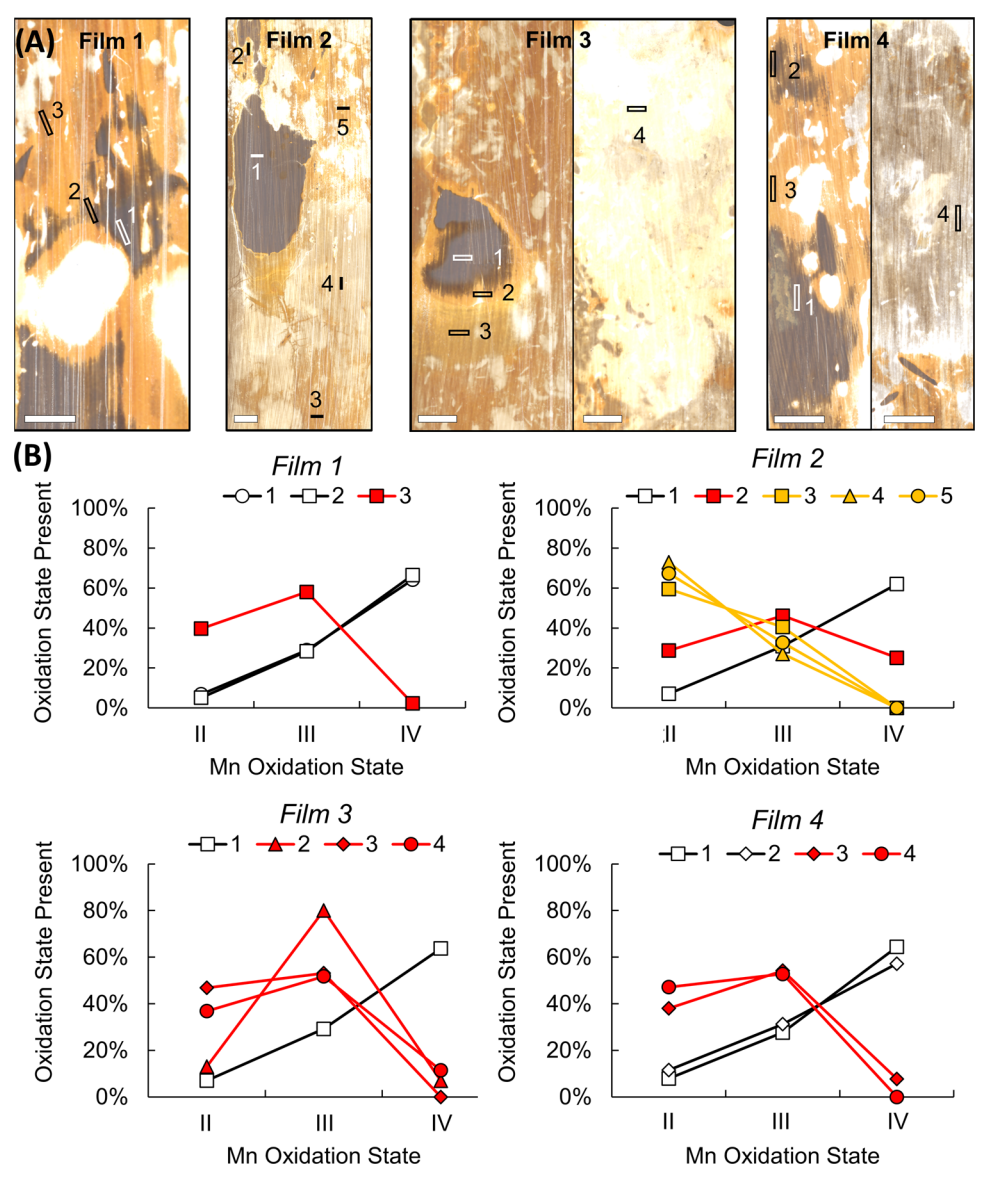


Figure 4. (A) Manganese IRIS films analyzed by Mn XANES, Mn EXAFS, and Fe EXAFS spectroscopy. Numbered rectangles denote the locations measured using a 5 mm × 1 mm beam (to scale). Films 3 and 4 each show two regions of an entire film that were analyzed. The full IRIS films are shown in Figure S1. The scale bar shown in white is 10 mm. (B) Mn XANES spectral linear combination fits for locations shown in panel A. Locations are colored according to the dominant Mn oxidation state present.

collected, although in some locations, insufficient Fe or Mn was present to perform LCF.

Manganese XANES spectra LCF revealed a partial reduction of Mn(IV) where Fe was apparent (Figures 4B and S5 and Table S3). On film 1, locations 1 and 2, both in Mn-rich areas, had Mn predominantly as Mn(IV). Location 3 had a mixture of Mn(II) and Mn(III). Film 2 was similar to film 1, although locations 3–5 were dominated by Mn(II). Both films 3 and 4 strongly resembled film 1, with Mn-rich areas containing Mn(IV), while other locations containing a mixture of Mn(II) and Mn(III). On film 3, location 2, located at the interface between the Mn-rich area and the Fe-rich area, contained a higher proportion of Mn(III) than all other locations.

Linear combination fitting of Mn EXAFS spectra followed two different approaches. First, the simplest model fit consisted of a nonreacted Mn IRIS film and Mn(II) adsorbed onto ferrihydrite. Note that despite performing adsorption anoxically, the Mn(II) partially oxidized to Mn(III) during

adsorption, resulting in an AOS of 2.23. This model adequately predicted the Mn EXAFS spectra for Mn-rich locations, finding that these locations could be completely modeled by the unexposed Mn IRIS film ($r \le 0.12$, Figure S6 and Table S4). This model fit poorly for areas where Mn XANES spectra revealed reduced Mn (r = 0.32 to 0.65). For these locations, additional Mn minerals were considered (see the Materials and Methods section), and rhodochrosite (MnCO₃) consistently outperformed other minerals. Including rhodochrosite into the LCF improved the fits for locations with reduced Mn ($r \le$ 0.20, Figure S6 and Table S4). For locations with reduced Mn, similar percentages of rhodochrosite and Mn(II) adsorbed to ferrihydrite were observed. The presence of rhodochrosite was confirmed by XRD and SEM (Figures S7 and S8) at several locations on different films where EXAFS spectra identified rhodochrosite.

Fe deposited on the Mn IRIS films was predominantly ferrihydrite, but lepidocrocite and goethite were also evident

(Figure S9 and Table S3). Linear combination fitting of Fe EXAFS spectra found that ferrihydrite ranged from 31 to 88% of the Fe (average \pm standard deviation: 65 \pm 20%, n = 10). Lepidocrocite and goethite comprised 17 \pm 11 and 19 \pm 15% of the Fe, respectively. The proportion of Fe minerals was compared to the Mn average oxidation state (Figure 5),

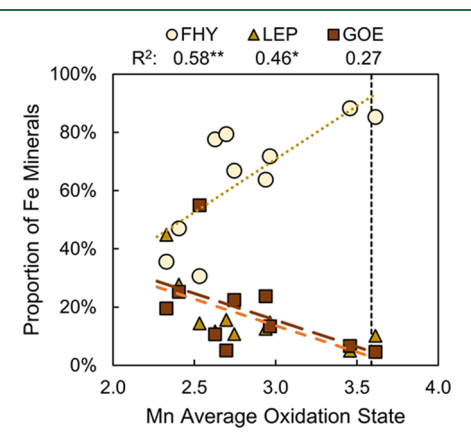


Figure 5. Correlations between the Mn average oxidation state and proportion of Fe minerals for locations shown in Figure 4A. Ferrihydrite (FHY) was the predominant mineral, although the fraction of FHY decreased with decreasing Mn AOS, resulting in higher fractions of lepidocrocite (LEP) and goethite (GOE). The vertical dashed line indicates the starting AOS for the Mn IRIS film. *p < 0.05; *p < 0.01.

revealing a positive correlation between Mn AOS and ferrihydrite (p=0.01) and a negative correlation between Mn AOS and lepidocrocite (p=0.03) and goethite (p=0.12). At low Mn AOS, there is some evidence of a nonlinear relationship, with some locations having higher lepidocrocite or goethite than predicted by the linear fit. However, there are insufficient data to develop a nonlinear model.

DISCUSSION

Fe Precipitation on Mn IRIS. Iron oxide precipitation on Mn IRIS devices can readily occur when Fe(II) is present in porewater. In this work, Fe precipitation occurred on most Mn films, although the distribution of Fe precipitates was heterogeneous (Figure S1). Even on small scales of <1 mm, the concentration of Fe and the Mn AOS varied substantially (Figures 1-3), making comparisons with porewater Fe, Mn, redox potential, and pH extremely difficult. In previous work under laboratory conditions, Mn IRIS exposed to solutions of 0.05, 5, 100, or 500 mg/L Fe(II) all accumulated Fe, but only the 500 mg/L treatment was noticeably and uniformly orange.²⁴ The authors also observed that the steady state was reached in \sim 1 day, indicating that Fe(II) oxidation by Mn IRIS is a relatively rapid process. The Fe(II) porewater concentrations in our work ranged from 20 to 35 mg/L Fe(II), lower than the 500 mg/L reported by Dorau and Mansfeldt² that resulted in an orange hue. However, Fe(II) concentrations in their experiment were not maintained throughout the exposure period since they report that Fe(II) "presumably auto-oxidized (by O₂) within 24 h." Regardless, the presence of orange deposits on a Mn IRIS device indicates that substantial amounts of Fe(II) were present in the porewater due to Fereducing conditions. For the purposes of the Hydric Soil Technical Standard, 11 Fe precipitation on Mn films should be

interpreted as evidence of reducing conditions because Fe reduction occurs at a lower redox potential than Mn reduction.

Laboratory studies of Fe(II) interactions with birnessite have shown similar patterns of mineral formation to those described here for Mn IRIS. When 1 g/L hexagonal birnessite was reacted with 20 mM Fe(II) under anoxic conditions, shortrange ordered Fe oxides were initially observed, with lepidocrocite detected after 2 h of contact time and goethite detected after 6 hours.³⁷ Birnessite was completely dissolved after 2 days.³⁷ In a column study, natural birnessite led to the precipitation of iron oxides and the release of Mn(II), although the release rate varied.³⁸ In diffusion-limited reactors, birnessite oxidized Fe(II) primarily into ferrihydrite with lesser amounts of lepidocrocite and goethite.³⁹

The neoformed Fe oxides on Mn IRIS present a valuable tool for studying (trans)formation dynamics and porewater interactions of Fe oxides. The formation of Fe oxides is often studied under laboratory conditions to enable careful manipulation of the experimental conditions and to allow retrieval of the reaction products. Such studies are rarely performed at field sites, yet new approaches such as Si wafers have been used to capture Fe oxides in field settings.40 Manganese IRIS can form Fe oxides under natural conditions, and these Fe oxides can be easily retrieved. Such Fe oxides are strong adsorbents of many contaminants and nutrients.⁴¹ The use of Mn IRIS to study neoformed Fe oxides has already shown that these minerals adsorbed and/or incorporated arsenic, phosphorous, manganese, organic matter, and lower amounts of chromium, zinc, and vanadium. 24,42 Because the neoformed Fe oxides are more representative of Fe oxides formed in situ than synthetic Fe oxides, we posit that Mn IRIS devices could be developed into passive samplers of solutes including As in natural environments. Note that the diversity of natural environments may result in the formation of additional Fe minerals on Mn IRIS, such as jarosite, schwertmannite, akageneite, feroxyhyte, and magnetite. Mn IRIS can also be used to study in situ Fe(II)-induced transformation of ferrihydrite to more crystalline phases such as lepidocrocite, goethite, and magnetite. 43,44 While Mn(II) can catalyze the transformation of ferrihydrite into more crystalline phases, transformation occurs more rapidly in the presence of Fe(II).³ Here, we found that the proportion of ferrihydrite was negatively correlated with Mn AOS (Figure 5), both of which are controlled by Fe(II). This suggests that areas of the film with more exposure to Fe(II) resulted in more complete reduction of Mn and more transformation of ferrihydrite to higher-ordered phases. These findings show that Mn IRIS can be used to map the variability in reducing conditions that arise due to physical and chemical complexity within a soil profile.

Mn Reduction by Fe(II). Manganese reductive dissolution can occur both biotically and abiotically. Biotic Mn reduction is presumed to be the dominant removal mechanism under Mn-reducing conditions, although Scott et al.²³ were unable to identify organisms or DNA present on exposed films. Because birnessite is a relatively strong oxidant under environmental conditions, abiotic reductive dissolution is possible. Romero et al.⁴⁵ showed that Mn IRIS can be reductively dissolved by dissolved sulfide but not dissolved organics. Ferrous iron can also reductively dissolve birnessite as shown in 1. Thus, the presence of reduced porewater constituents can lead to Mn coating removal over timescales of interest.

Birnessite is well-known to oxidize Fe(II). In laboratory experiments, increased Fe(II) concentrations increased rates of

birnessite reduction, but the reaction slowed as pH increased toward neutral. 37,46 Similarly, reactors with more MnO₂ resulted in more Fe(II) oxidation.⁴⁷ The fate of the Mn oxides in the presence of Fe(II) can vary. In diffusion-limited reactors, birnessite AOS reduced from 3.9 to 3.1, and this reduction was more substantial in reactors with less Fe(II) added.³⁹ The authors hypothesized that Mn(II) was associated with the mineral rather than had diffused away from the mineral. In anoxic experiments without Fe, the interaction of birnessite and Mn(II) formed feitknechtite (β -Mn(III)OOH) through comproportionation at low Mn(II) concentrations (\leq 600 μ M) and manganite (γ -Mn(III)OOH) at high Mn(II) concentrations (600–4000 μ M). In laboratory experiments, birnessite oxidized As(III) through two-electron transfer reaction, resulting in Mn(II), which later formed Mn(III) through comproportionation.⁴⁹ In our work, we observed extensive reduction of Mn in some locations, with Mn AOS falling below 2.5 (Figure 5). While we observed Mn(III) in Mn XANES spectra (Figures 1–3 and 5), Mn EXAFS spectroscopy did not reveal the presence of any Mn(III) minerals such as feitknechtite or Mn(III) substituted into iron oxides (Table S4), perhaps due to the relatively high percentage of Mn(III) in the synthesized birnessite (35%, Table S3). Thus, much of the Mn(III) may still be present as birnessite but with a lower average oxidation state, since birnessite can contain appreciable amounts of Mn(III). 50 Note that the Mn(II) adsorbed to ferrihydrite standard also contained some Mn(III), with an Mn AOS of 2.23. Additionally, the fate of Mn(II) in soils can vary from reactor experiments with synthetic minerals due to the presence of other dissolved constituents, making direct comparisons between field and laboratory results difficult.

This work provides evidence for the fate of the reduced Mn after dissolution from birnessite, particularly for disequilibrium systems such as IRIS in soils. If the Mn(II) diffused away from the IRIS film and did not interact with the remaining minerals on the IRIS film, the Mn AOS would be expected to remain near 3.6—the value of a Mn IRIS film not exposed to reducing conditions (Figure 6). Instead, we observed lower Mn AOS in all locations where the Mn IRIS film exhibited a color change. In such locations, both bulk XANES and μ XANES spectroscopy showed Mn on the IRIS film was predominantly Mn(II/ III) (Figures 1-3C and 4B). This suggests that the reduced Mn either adsorbed onto other minerals or formed reduced Mn minerals. Because oxidized Fe was present with reduced Mn, adsorption of Mn(II) onto ferrihydrite is possible.³⁷ However, we observed poor linear combination fits of Mn EXAFS spectra when considering a model with only the nonreacted Mn IRIS film and Mn(II) adsorbed onto ferrihydrite for locations with reduced Mn, indicating a missing Mn(II/III) component (Table S4 and Figure S6). Additionally, the adsorption capacity of ferrihydrite for Mn(II) is ~ 0.04 mol Mn(II)/mol ferrihydrite, 51 which assumes no other competing sorbates and places an upper bound on the amount of Mn(II) that could be adsorbed by ferrihydrite given 1, in which 1 mole of Mn(II) is formed for every 2 moles of Fe(II) oxidized (orange dashed line on Figure 6). The μ XRF and μ XANES spectra show that, despite the decrease in Mn AOS, the concentration of Mn can exceed the theoretical adsorption capacity of ferrihydrite, indicating Mn is likely precipitating as another reduced Mn compound (Figure 6). The Fe-rich areas in the μ XRF images also show Mn remaining, although 1-4 orders of magnitude in Mn removal is apparent (Figures 1–3D). Of the Mn(II) minerals examined for the Mn EXAFS

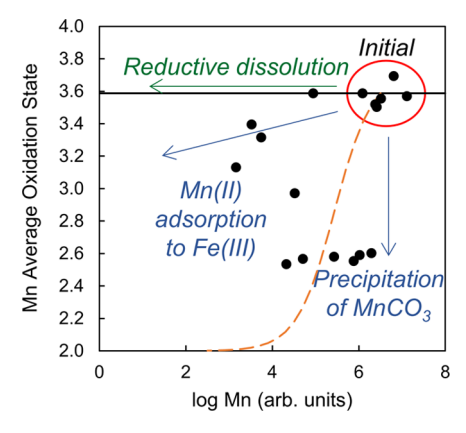


Figure 6. Conceptual model of Mn reductive dissolution on Mn IRIS films. Locations in the upper right corner labeled "Initial" are Mn-rich locations characteristic of an initial Mn IRIS film. Oxidized Mn can be (1) reductively dissolved from the film, which would decrease Mn concentration at constant Mn AOS unless (2) reduced Mn adsorbed to ferrihydrite and/or (3) reduced Mn reprecipitated on the film as rhodochrosite. The solid black line indicates the Mn AOS for an initial film. The dashed orange line represents the sorption capacity of Mn(II) on ferrihydrite of 0.04 mol/mol assuming that 1 mol of Mn(II) produced 2 mol of ferrihydrite and no competing sorbates. Actual films demonstrated all three mechanisms as shown by black dots, which are locations where μ -XANES spectroscopy was performed.

spectra fitting, rhodochrosite provided a drastic improvement in fit, showing similar fractions of Mn(II) adsorbed to ferrihydrite and rhodochrosite (Table S4 and Figure S6). The presence of rhodochrosite was verified by XRD and SEM (Figures S7 and S8). Rhodochrosite (MnCO₃) is sparingly soluble ($K_{\rm sp}=2.60\times10^{-11}$), S2 requiring relatively low concentrations of carbonate adjacent to the film where Mn(II) concentrations are locally elevated. Because of this, rhodochrosite is the dominant Mn(II) mineral phase in neutral to alkaline anoxic environments. 53,54 Geochemical modeling has found supersaturation of rhodochrosite in rice soil incubations, particularly under neutral to alkaline pH.55,56 Note that the soil was flooded during IRIS film deployment, and the slightly acidic soil pH moved toward neutral in porewater or slightly alkaline, providing sufficient pH conditions for rhodochrosite formation. The presence of a dense rooting system by rice also provided elevated CO2 due to root respiration, providing a source of bicarbonate to the system. Moreover, rhodochrosite is also formed by Mn-reducing bacteria because Mn(III/IV) reduction coupled to carbon oxidation produces bicarbonate and consumes protons. ^{57–60} Collectively, the data suggest that the introduction of birnessite and Mn reduction in the flooded rice paddy can result in local areas of elevated porewater bicarbonate, pH, and Mn(II) that results in the formation of rhodochrosite.

Of practical interest when interpreting Mn IRIS, most of the Mn is removed under reducing conditions regardless of the exact mechanism. We did not focus on locations where substantial reductive dissolution occurred because insufficient Mn remained to perform Mn XAS. In the μ XRF work, Mn signal intensity decreased by 1–4 orders of magnitude in the Fe-rich areas relative to the Mn-rich areas (Figures 1–3D), demonstrating that Fe(II) can effectively remove large quantities of Mn from the film. Reductive dissolution of Mn is likely also occurring through Mn-reducing bacteria, which would encourage the precipitation of rhodochrosite, partic-

ularly if plant roots are present. If rhodochrosite remaining on the IRIS film is measured by chemical extraction or XRF, the reduced Mn present on the film could be incorrectly interpreted as birnessite and a lack of evidence of reducing conditions. Rhodochrosite has also been reported to undergo relatively rapid oxidation in the presence of goethite into groutite under oxic conditions, 61 so the fate of rhodochrosite may vary if redox conditions vary. However, note that in the conditions encountered in this work, even in locations with reduced Mn present on the film, Mn concentrations were often substantially lower than in areas without reduced Mn (Figure 6). Furthermore, large sections of the films were white, indicative of complete removal of the Mn coating. Whether this occurred directly through reductive dissolution of Mn or through a two-step reductive dissolution of Mn by Fe(II) and then reductive dissolution of Fe is unclear. Regardless, we recommend that practitioners of Mn IRIS consider areas of Fe precipitation to be taken as evidence of reducing conditions analogous to Mn coating removal.

The extensive spatial heterogeneity observed on all films highlights the potential use of IRIS to better understand the kinetics of redox reactions in soils. While we expected biotic or abiotic removal of the Mn coating, we observed some locations where neither occurred, perhaps due to a zone of oxygenation due to preferential flow paths connecting the surface to the subsurface. In other areas, Fe precipitation was evident as Fe(II) reduced birnessite, precipitating as ferrihydrite. Continued exposure to Fe(II) likely further reduced birnessite and transformed ferrihydrite into lepidocrocite and goethite. 43,44 The fate of Mn(II) varied, perhaps due to local differences in biogeochemistry, with some Mn(II) diffusing away from the film, some adsorbing onto ferrihydrite, and some precipitating as rhodochrosite. In other locations, no coating was present due to a complete reduction of metal oxides from the film. Studying such variability requires obtaining spatially resolved data, which IRIS is particularly well suited to provide, perhaps in combination with other spatially resolved measurements of biogeochemistry. 62 While the fate of birnessite can vary depending on specific porewater chemistry, this work describes several mechanisms and demonstrates the use of Mn IRIS to study the transformation and fate of birnessite under field conditions.

ASSOCIATED CONTENT

Supporting Information

The Supporting Information is available free of charge at https://pubs.acs.org/doi/10.1021/acs.est.3c00161.

Additional Fe and Mn false color μ XRF images, XANES spectra and fits, EXAFS spectra and fits, XRD diffractograms, SEM images, porewater chemistry, and description of the synthesis of Mn(III) lepidocrocite and Mn(III) goethite (PDF)

Normalized spectra for bulk Fe XAS samples and standards (TXT)

Normalized spectra for bulk Mn XAS samples and standards (TXT)

AUTHOR INFORMATION

Corresponding Author

Angelia L. Seyfferth – Department of Plant and Soil Science, University of Delaware, Newark, Delaware 19716, United States; orcid.org/0000-0003-3589-6815; Email: angelias@udel.edu

Authors

Matt A. Limmer — Department of Plant and Soil Science, University of Delaware, Newark, Delaware 19716, United States; orcid.org/0000-0001-8119-0229

Franklin A. Linam — Department of Plant and Soil Science, University of Delaware, Newark, Delaware 19716, United States; orcid.org/0000-0001-5071-1300

Abby E. Evans – Department of Plant and Soil Science, University of Delaware, Newark, Delaware 19716, United States

Complete contact information is available at: https://pubs.acs.org/10.1021/acs.est.3c00161

Notes

The authors declare no competing financial interest.

ACKNOWLEDGMENTS

This research was funded by the National Science Foundation (Grant #1930806) and the U.S. Department of Agriculture National Institute of Food and Agriculture (Grant #2018-67019-27796). Use of the Stanford Synchrotron Radiation Lightsource, SLAC National Accelerator Laboratory, is supported by the US Department of Energy, Office of Science, Office of Basic Energy Sciences under Contract No. DE-AC02-76SF00515. This research used beamline 6-BM of the National Synchrotron Light Source II, a US Department of Energy (DOE) Office of Science User Facility operated for the DOE Office of Science by Brookhaven National Laboratory under Contract No. DE-SC0012704.

REFERENCES

- (1) Borch, T.; Kretzschmar, R.; Kappler, A.; van Cappellen, P.; Ginder-Vogel, M.; Voegelin, A.; Campbell, K. Biogeochemical Redox Processes and Their Impact on Contaminant Dynamics. *Environ. Sci. Technol.* **2010**, *44*, 15–23.
- (2) Fiedler, S.; Vepraskas, M. J.; Richardson, J. L. Soil Redox Potential: Importance, Field Measurements, and Observations. *Adv. Agron.* **2007**, *94*, 1–54.
- (3) Cornell, R. M.; Schwertmann, U. Solubility. In *The Iron Oxides:* Structure, Properties, Reactions, Occurrences and Uses; John Wiley & Sons, Inc.: New York, NY, 2006; pp 201–220.
- (4) Castenson, K. L.; Rabenhorst, M. C. Indicator of Reduction in Soil (IRIS). Soil Sci. Soc. Am. J. 2006, 70, 1222–1226.
- (5) Jenkinson, B. J.; Franzmeier, D. P. Development and Evaluation of Iron-Coated Tubes That Indicate Reduction in Soils. *Soil Sci. Soc. Am. J.* **2006**, *70*, 183–191.
- (6) Sapkota, Y.; Duball, C.; Vaughan, K.; Rabenhorst, M. C.; Berkowitz, J. F. Indicator of Reduction in Soil (IRIS) Devices: A Review. *Sci. Total Environ.* **2022**, *852*, No. 158419.
- (7) Rabenhorst, M. C.; Burch, S. N. Synthetic Iron Oxides as an Indicator of Reduction in Soils (IRIS). *Soil Sci. Soc. Am. J.* **2006**, *70*, 1227–1236.
- (8) Rabenhorst, M. C. Simple and Reliable Approach for Quantifying IRIS Tube Data. Soil Sci. Soc. Am. J. 2012, 76, 307–308.
- (9) Rabenhorst, M. C. Protocol for Using and Interpreting IRIS Tubes. *Soil Horiz.* **2008**, 49, 74–77.
- (10) Limmer, M. A.; Evans, A. E.; Seyfferth, A. L. The IRIS Imager: A Freeware Program for Quantification of Paint Removal on IRIS Films. *Soil Sci. Soc. Am. J.* **2021**, *85*, 2210–2219.
- (11) Berkowitz, J. F.; Vepraskas, M. J.; Vaughan, K. L.; Vasilas, L. M. Development and Application of the Hydric Soil Technical Standard. *Soil Sci. Soc. Am. J.* **2021**, *85*, 469–487.

- (12) Duball, C.; Vaughan, K.; Berkowitz, J. F.; Rabenhorst, M. C.; VanZomeren, C. M. Iron Monosulfide Identification: Field Techniques to Provide Evidence of Reducing Conditions in Soils. *Soil Sci. Soc. Am. J.* **2020**, *84*, 303–313.
- (13) Rabenhorst, M. C.; Megonigal, J. P.; Keller, J. Synthetic Iron Oxides for Documenting Sulfide in Marsh Pore Water. *Soil Sci. Soc. Am. J.* **2010**, *74*, 1383–1388.
- (14) Rabenhorst, M. C.; Persing, K. A. A Synthesized Manganese Oxide for Easily Making Durable Manganese-Coated IRIS Tubes. *Soil Sci. Soc. Am. J.* **2017**, *81*, 233–239.
- (15) Dorau, K.; Mansfeldt, T. Manganese-Oxide-Coated Redox Bars as an Indicator of Reducing Conditions in Soils. *J. Environ. Qual.* **2015**, *44*, 696–703.
- (16) Stiles, C. A.; Dunkinson, E. T.; Ping, C.-L.; Kidd, J. Initial Field Installation of Manganese Indicators of Reduction in Soils, Brooks Range, Alaska. *Soil Horiz.* **2010**, *51*, 102–107.
- (17) Rabenhorst, M. C.; Post, J. Manganese Oxides for Environmental Assessment. Soil Sci. Soc. Am. J. 2018, 82, 509-518.
- (18) Dorau, K.; Eickmeier, M.; Mansfeldt, T. Comparison of Manganese and Iron Oxide-Coated Redox Bars for Characterization of the Redox Status in Wetland Soils. *Wetlands* **2016**, *36*, 133–141.
- (19) Rabenhorst, M. C.; Drohan, P. J.; Galbraith, J. M.; Moorberg, C.; Spokas, L.; Stolt, M. H.; Thompson, J. A.; Turk, J.; Vasilas, B. L.; Vaughan, K. L. Manganese-Coated IRIS to Document Reducing Soil Conditions. *Soil Sci. Soc. Am. J.* **2021**, *85*, 2201–2209.
- (20) Dorau, K.; Papenfuß, S.; Mansfeldt, T. Temperature-Dependent Oxide Removal from Manganese- and Iron Oxide-Coated Soil Redox Bars. *J. Soils Sediments* **2018**, *18*, 680–687.
- (21) Evans, A. E.; Limmer, M. A.; Seyfferth, A. L. Indicator of Redox in Soil (IRIS) Films as a Water Management Tool for Rice Farmers. *J. Environ. Manage.* **2021**, 294, No. 112920.
- (22) Krishnamurti, G. S. R.; Huang, P. M. The Catalytic Role of Birnessite in the Transformation of Iron. *Can. J. Soil Sci.* **1987**, *67*, 533–543.
- (23) Scott, B.; Baldwin, A. H.; Yarwood, S.; Castañeda, C.; Latorre, B.; Rabenhorst, M. C. Macro and Microscopic Visual Imaging Tools to Investigate Metal Reducing Bacteria in Soils. *Soil Sci. Soc. Am. J.* **2021**, *85*, 184–192.
- (24) Dorau, K.; Mansfeldt, T. Manganese and Iron Oxide-Coated Redox Bars as a Tool to in Situ Study the Element Sorption in Wet Soils. *J. Soils Sediments* **2016**, *16*, 976–986.
- (25) Limmer, M. A.; Evans, A. E.; Seyfferth, A. L. A New Method to Capture the Spatial and Temporal Heterogeneity of Aquatic Plant Iron Root Plaque *in situ. Environ. Sci. Technol.* **2021**, *55*, 912–918.
- (26) Limmer, M. A.; Thomas, J.; Seyfferth, A. L. The Effect of Silicon on the Kinetics of Rice Root Iron Plaque Formation. *Plant Soil* **2022**, *477*, 171–181.
- (27) Rabenhorst, M. C. A System for Making and Deploying Oxide-Coated Plastic Films for Environmental Assessment of Soils. *Soil Sci. Soc. Am. J.* **2018**, 82, 1301–1307.
- (28) Limmer, M. A.; Mann, J.; Amaral, D. C.; Vargas, R.; Seyfferth, A. L. Silicon-Rich Amendments in Rice Paddies: Effects on Arsenic Uptake and Biogeochemistry. *Sci. Total Environ.* **2018**, *624*, 1360–1368.
- (29) Limmer, M. A.; Seyfferth, A. L. Carryover Effects of Silicon-rich Amendments in Rice Paddies. *Soil Sci. Soc. Am. J.* **2021**, *85*, 314–327.
- (30) Wenzel, W. W.; Kirchbaumer, N.; Prohaska, T.; Stingeder, G.; Lombi, E.; Adriano, D. C. Arsenic Fractionation in Soils Using an Improved Sequential Extraction Procedure. *Anal. Chim. Acta* **2001**, 436, 309–323.
- (31) Gambrell, R. P. Manganese. In Methods of Soil Analysis: Part 3 Chemical Methods; Sparks, D. L., Ed.; Soil Science Society of America, 1996; pp 665–682.
- (32) Stookey, L. L. Ferrozine—a New Spectrophotometric Reagent for Iron. *Anal. Chem.* **1970**, 42, 779–781.
- (33) Webb, S. M.; McNulty, I.; Eyberger, C.; Lai, B. The MicroAnalysis Toolkit: X-Ray Fluorescence Image Processing Software. *AIP Conf. Proc.* **2011**, *1365*, 196–199.

- (34) Manceau, A.; Marcus, M. A.; Grangeon, S. Determination of Mn Valence States in Mixed-Valent Manganates by XANES Spectroscopy. *Am. Mineral.* **2012**, *97*, 816–827.
- (35) Ahmad, A.; van der Wal, A.; Bhattacharya, P.; van Genuchten, C. M. Characteristics of Fe and Mn Bearing Precipitates Generated by Fe(II) and Mn(II) Co-Oxidation with O₂ MnO₄ and HOCl in the Presence of Groundwater Ions. *Water Res.* **2019**, *161*, 505–516.
- (36) Vempati, R. K.; Morris, R. V.; Lauer, H. V.; Helmke, P. A. Reflectivity and Other Physicochemical Properties of Mn-Substituted Goethites and Hematites. *J. Geophys. Res.* **1995**, *100*, 3285–3295.
- (37) Gao, T.; Shen, Y.; Jia, Z.; Qiu, G.; Liu, F.; Zhang, Y.; Feng, X.; Cai, C. Interaction Mechanisms and Kinetics of Ferrous Ion and Hexagonal Birnessite in Aqueous Systems. *Geochem. Trans.* **2015**, *16*, No. 16.
- (38) Postma, D.; Appelo, C. A. J. Reduction of Mn-Oxides by Ferrous Iron in a Flow System: Column Experiment and Reactive Transport Modeling. *Geochim. Cosmochim. Acta* **2000**, *64*, 1237–1247.
- (39) Mock, R. P.; Schaefer, Mv.; Pacheco, J. L.; Lake, L.; Lee, I.; Ying, S. C. Influence of Fe(II) on Arsenic(III) Oxidation by Birnessite in Diffusion-Limited Systems. *ACS Earth Space Chem.* **2019**, *3*, 550–561.
- (40) Rennert, T.; Mueller, C. W.; Mansfeldt, T.; Lugmeier, J. Collecting *in situ* Precipitated Iron Oxides in Their Natural Soil Environment. *J. Plant Nutr. Soil Sci.* **2013**, *176*, 497–499.
- (41) Cornell, R. M.; Schwertmann, U. Adsorption of Ions and Molecules. In *The Iron Oxides: Structure, Properties, Reactions, Occurrences and Uses*; John Wiley & Sons, Inc.: New York, NY, 2006; pp 253–296 DOI: 10.1002/3527602097.ch11.
- (42) Dorau, K.; Pohl, L.; Just, C.; Höschen, C.; Ufer, K.; Mansfeldt, T.; Mueller, C. W. Soil Organic Matter and Phosphate Sorption on Natural and Synthetic Fe Oxides under in Situ Conditions. *Environ. Sci. Technol.* **2019**, *53*, 13081–13087.
- (43) Hansel, C. M.; Benner, S. G.; Fendorf, S. Competing Fe(II)-Induced Mineralization Pathways of Ferrihydrite. *Environ. Sci. Technol.* **2005**, *39*, 7147–7153.
- (44) Boland, D. D.; Collins, R. N.; Miller, C. J.; Glover, C. J.; Waite, T. D. Effect of Solution and Solid-Phase Conditions on the Fe(II)-Accelerated Transformation of Ferrihydrite to Lepidocrocite and Goethite. *Environ. Sci. Technol.* **2014**, *48*, 5477–5485.
- (45) Romero, J.; Hino, K.; Loffredo, J.; Stolt, M.; Moseman-Valtierra, S.; Amador, J.; Pellock, B. Abiotic Soil Properties Affecting Interpretation of IRIS Sensors in Tidal and Freshwater Soils. *Soil Sci. Soc. Am. J.* **2021**, *85*, 2234–2239.
- (46) Postma, D. Concentration of Mn and Separation from Fe in Sediments I. Kinetics and Stoichiometry of the Reaction between Birnessite and Dissolved Fe(II) at 10 $^{\circ}$ C. *Geochim. Cosmochim. Acta* 1985, 49, 1023–1033.
- (47) He, Y. T.; Hering, J. G. Enhancement of Arsenic(III) Sequestration by Manganese Oxides in the Presence of Iron(II). *Water, Air, Soil Pollut.* **2009**, 203, 359–368.
- (48) Elzinga, E. J. Reductive Transformation of Birnessite by Aqueous Mn(II). *Environ. Sci. Technol.* **2011**, *45*, 6366–6372.
- (49) Wu, Y.; Kukkadapu, R. K.; Livi, K. J. T.; Xu, W.; Li, W.; Sparks, D. L. Iron and Arsenic Speciation during As(III) Oxidation by Manganese Oxides in the Presence of Fe(II): Molecular-Level Characterization Using XAFS, Mössbauer, and TEM Analysis. ACS Earth Space Chem. 2018, 2, 256–268.
- (50) Remucal, C. K.; Ginder-Vogel, M. A Critical Review of the Reactivity of Manganese Oxides with Organic Contaminants. *Environ. Sci. Process Impacts* **2014**, *16*, 1247–1266.
- (51) Lan, S.; Wang, X.; Xiang, Q.; Yin, H.; Tan, W.; Qiu, G.; Liu, F.; Zhang, J.; Feng, X. Mechanisms of Mn(II) Catalytic Oxidation on Ferrihydrite Surfaces and the Formation of Manganese (Oxyhydr)-Oxides. *Geochim. Cosmochim. Acta* **2017**, 211, 79–96.
- (52) Johnson, K. S. Solubility of Rhodochrosite (MnCO₃) in Water and Seawater. *Geochim. Cosmochim. Acta* 1982, 46, 1805–1809.

- (53) Lebron, I.; Suarez, D. L. Mechanisms and Precipitation Rate of Rhodochrosite at 25 °C as Affected by P_{CO2} and Organic Ligands. *Soil Sci. Soc. Am. J.* **1999**, 63, 561–568.
- (54) Li, Y.; Wang, X.; Li, Y.; Duan, J.; Jia, H.; Ding, H.; Lu, A.; Wang, C.; Nie, Y.; Wu, X. Coupled Anaerobic and Aerobic Microbial Processes for Mn-Carbonate Precipitation: A Realistic Model of Inorganic Carbon Pool Formation. *Geochim. Cosmochim. Acta* **2019**, 256, 49–65.
- (55) Maguffin, S. C.; Abu-Ali, L.; Tappero, Rv.; Pena, J.; Rohila, J. S.; McClung, A. M.; Reid, M. C. Influence of Manganese Abundances on Iron and Arsenic Solubility in Rice Paddy Soils. *Geochim. Cosmochim. Acta* **2020**, 276, 50–69.
- (56) Pan, Y.; Koopmans, G. F.; Bonten, L. T. C.; Song, J.; Luo, Y.; Temminghoff, E. J. M.; Comans, R. N. J. Influence of PH on the Redox Chemistry of Metal (Hydr)Oxides and Organic Matter in Paddy Soils. *J. Soils Sediments* **2014**, *14*, 1713–1726.
- (57) Lovley, D. R.; Phillips, E. J. P. Novel Mode of Microbial Energy Metabolism: Organic Carbon Oxidation Coupled to Dissimilatory Reduction of Iron or Manganese. *Appl. Environ. Microbiol.* **1988**, *54*, 1472–1480.
- (58) Lovley, D. R. Dissimilatory Fe(III) and Mn(IV) Reduction. *Microbiol. Rev.* **1991**, 55, 259–287.
- (59) Nealson, K. H.; Saffarini, D. Iron and Manganese in Anaerobic Respiration: Environmental Significance, Physiology, and Regulation. *Annu. Rev. Microbiol.* **1994**, *48*, 311–354.
- (60) Lovley, D. R.; Phillips, E. J. P.; Lonergan, D. J. Hydrogen and Formate Oxidation Coupled to Dissimilatory Reduction of Iron or Manganese by *Alteromonas putrefaciens*. *Appl. Environ. Microbiol.* **1989**, 55, 700–706.
- (61) Namgung, S.; Lee, G. Rhodochrosite Oxidation by Dissolved Oxygen and the Formation of Mn Oxide Product: The Impact of Goethite as a Foreign Solid Substrate. *Environ. Sci. Technol.* **2021**, *55*, 14436–14444.
- (62) Dorau, K.; Uteau, D.; Maisch, M.; Kappler, A.; Peth, S.; Mansfeldt, T. Redoxtrons An Experimental System to Study Redox Processes within the Capillary Fringe. *Eur. J. Soil Sci.* **2023**, *74*, No. e13347.

□ Recommended by ACS

Fe(II)-Catalyzed Transformation of Ferrihydrite with Different Degrees of Crystallinity

Yuyan Liu, Juan Liu, et al.

APRIL 20, 2023

ENVIRONMENTAL SCIENCE & TECHNOLOGY

READ 🗹

Antimony Isotope Fractionation Revealed from EXAFS during Adsorption on Fe (Oxyhydr)oxides

Weiqing Zhou, Xin Liu, et al.

JUNE 09, 2023

ENVIRONMENTAL SCIENCE & TECHNOLOGY

READ 🗹

Reductive Sequestration of Cr(VI) and Immobilization of C during the Microbially Mediated Transformation of Ferrihydrite-Cr(VI)-Fulvic Acid Coprecipitates

Shiwen Hu, Chongxuan Liu, et al.

MAY 22, 2023

ENVIRONMENTAL SCIENCE & TECHNOLOGY

READ [7

Iron Vacancy Accelerates Fe(II)-Induced Anoxic As(III) Oxidation Coupled to Iron Reduction

Liping Fang, Fangbai Li, et al.

JANUARY 24, 2023

ENVIRONMENTAL SCIENCE & TECHNOLOGY

READ 🗹

Get More Suggestions >